Jupiter's formation and its primordial internal structure

Lozovsky, Michael ; Helled, Ravit ; Rosenberg, Eric D ; Bodenheimer, Peter

Abstract: The composition of Jupiter and the primordial distribution of the heavy elements are determined by its formation history. As a result, in order to constrain the primordial internal structure of Jupiter, the growth of the core and the deposition and settling of accreted planetesimals must be followed in detail. In this paper we determine the distribution of the heavy elements in proto-Jupiter and determine the mass and composition of the core. We find that while the outer envelope of proto-Jupiter is typically convective and has a homogeneous composition, the innermost regions have compositional gradients. In addition, the existence of heavy elements in the envelope leads to much higher internal temperatures (several times 104 K) than in the case of a hydrogen–helium envelope. The derived core mass depends on the actual definition of the core: if the core is defined as the region in which the heavy-element mass fraction is above some limit (say, 0.5), then it can be much more massive (15 $M_{\oplus}$) and more extended (10% of the planet's radius) than in the case where the core is just the region with 100% heavy elements. In the former case Jupiter's core also consists of hydrogen and helium. Our results should be taken into account when constructing internal structure models of Jupiter and when interpreting the upcoming data from the Juno (NASA) mission.

DOI: https://doi.org/10.3847/1538-4357/836/2/227

The Astrophysical Journal, 836:227 (16pp), 2017 February 20 doi:10.3847/1538-4357/836/2/227

Jupiter's Formation and Its Primordial Internal Structure

Michael Lozovsky[1,2], Ravit Helled[1,2], Eric D. Rosenberg[1], and Peter Bodenheimer[3]
[1] Department of Geosciences, Tel-Aviv University, Tel-Aviv, Israel
[2] Center for Theoretical Astrophysics & Cosmology, Institute for Computational Science, University of Zurich, Zurich, Switzerland
[3] UCO/Lick Observatory, University of California Santa Cruz, USA
Received 2016 October 28; revised 2016 December 31; accepted 2017 January 3; published 2017 February 22

Abstract

The composition of Jupiter and the primordial distribution of the heavy elements are determined by its formation history. As a result, in order to constrain the primordial internal structure of Jupiter, the growth of the core and the deposition and settling of accreted planetesimals must be followed in detail. In this paper we determine the distribution of the heavy elements in proto-Jupiter and determine the mass and composition of the core. We find that while the outer envelope of proto-Jupiter is typically convective and has a homogeneous composition, the innermost regions have compositional gradients. In addition, the existence of heavy elements in the envelope leads to much higher internal temperatures (several times 10^4 K) than in the case of a hydrogen–helium envelope. The derived core mass depends on the actual definition of the core: if the core is defined as the region in which the heavy-element mass fraction is above some limit (say, 0.5), then it can be much more massive ($\sim$15 $M_\oplus$) and more extended (10% of the planet's radius) than in the case where the core is just the region with 100% heavy elements. In the former case Jupiter's core also consists of hydrogen and helium. Our results should be taken into account when constructing internal structure models of Jupiter and when interpreting the upcoming data from the *Juno* (NASA) mission.

Key words: planets and satellites: composition – planets and satellites: formation – planets and satellites: gaseous planets – planets and satellites: individual (Jupiter) – planets and satellites: interiors

1. Introduction

In the standard model for giant planet formation, core accretion (CA), the formation of a gaseous planet begins with the growth of a heavy-element core (e.g., Pollack et al. 1996; Alibert et al. 2005). The exact mass and composition of the core are unknown, but it is commonly agreed that it should be of the order of at least several Earth masses ($M_\oplus$) in order to allow the follow-up of gas accretion. The core's composition is assumed to be rocky and/or icy. Giant planet formation models also typically assume that the accreted solid material (planetesimals) falls all the way to the center, increasing the core's mass. Indeed, at the beginning of their formation, giant planets are capable of binding only a very tenuous envelope, so that infalling planetesimals essentially reach the core directly, but as the growing planet accretes a gaseous atmosphere, the planetesimals do not necessarily reach the core, but instead dissolve in the gaseous envelope.

A major science objective in giant planet studies is to relate the observed planetary structure to the origin and evolution of the planet. For years now, the existence of a heavy-element (high-Z) core and/or enriched envelope has been taken as support of the CA model. The connection between planetary origin and internal structure, however, is nontrivial, and in fact, different formation mechanisms and birth environments lead to a large range of compositions and internal structures (e.g., Helled et al. 2014). Even within the CA framework, the primordial internal structures of the planets are not well constrained. For giant exoplanets, an estimate of the total mass of heavy elements in the planet is sufficient for planetary characterization because (at present) it is difficult to constrain the heavy-element distribution. A possible approach to this question employs the tidal Love number and is applied to the exoplanet HAT-P 13b by Kramm et al. (2012) and Buhler et al. (2016). This is different for the case of Jupiter, for which we have accurate measurements of the gravitational field, and therefore estimates of its internal density distribution can be determined.

In this paper, we determine the heavy-element distribution and core mass in proto-Jupiter at different stages during its formation in the CA model. We follow the accreted planetesimals as they enter the planetary envelope and determine their distribution accounting for settling and convective mixing. Formation models with different solid-surface densities and planetesimal sizes are considered, as well as different definitions of the planetary core. This work aims to provide a more complete theoretical framework for the interpretation of *Juno* data. The initial orbit insertion of the *Juno* (NASA) spacecraft was on July 4. *Juno* will measure Jupiter's gravitational moments J_n and atmospheric composition below the cloud level (e.g., Helled & Lunine 2014). These measurements will provide tighter constraints on Jupiter's density distribution, and hence its internal structure, with the aim of using this information to better understand Jupiter's origin. In order to link Jupiter's internal structure and formation history, we first need to understand what is the expected internal structure from formation models, as well as its sensitivity to the various model assumptions. This work aims to explore and put limits on the primordial internal structure of Jupiter, in particular, its core properties.

2. Methods and Model Assumptions

2.1. Planet Formation Models

In order to determine the heavy-element distribution in proto-Jupiter, we use four giant planet formation models, whose properties are summarized in Table 1. Models are produced using the standard core accretion code described in Pollack et al. (1996) and updated by Lissauer et al. (2009).

Table 1
Properties of the Four Baseline Formation Models

Formation Model	σ (g cm^{-2})	Planetesimal Size (km)	$M_{\rm core}$ at Crossover Time ($M_\oplus$)	Crossover Time (Myr)
Model A	6	100	7.5	1.54
Model B	6	0.5	7.6	1.33
Model C	10	1	15.7	0.90
Model D	10	100	16.0	0.94

Model D is the model with solid-surface density $\sigma = 10\,{\rm g\,cm^{-2}}$ described by Movshovitz et al. (2010). In this model, the grain opacities were determined through detailed simulations of grain settling and coagulation. In models A through C, the grain opacities were determined approximately as a fraction $f \ll 1$ of interstellar opacities, with f adjusted to reproduce the formation times found by Movshovitz et al. for $\sigma = 10\,{\rm g\,cm^{-2}}$ and $\sigma = 6\,{\rm g\,cm^{-2}}$. The formation models provide the distribution of the physical properties of the planetary envelope, such as the temperature T, pressure P, luminosity L, opacity κ, mass M, and the total mass of gas (hydrogen and helium in protosolar ratio) and the total mass of heavy elements as a function of time.

These formation models are derived under the assumption that all the planetesimals settle to the center and join the core, and the inferred crossover time and crossover mass (mass of solids equals the mass of hydrogen–helium gas $M_Z = M_{\rm H+He}$) correspond to the model under this assumption. If the heavy elements are allowed to stay in the envelope and are accounted for self-consistently in the formation model, the formation history, and therefore also crossover mass and crossover time, is expected to change as well.

As can be seen from the table, the formation timescale and the core mass are sensitive to the assumed solid-surface densities and planetesimal sizes (e.g., Pollack et al. 1996; Movshovitz et al. 2010). Higher solid-surface density σ and smaller planetesimal sizes lead to faster growth. The crossover time for the different models ranges between 0.9 and 1.5 Myr. These timescales, however, are calculated for envelopes that are metal-free, the time to reach crossover is expected to be shorter if the heavy elements are taken into account in the calculation (e.g., Hori & Ikoma 2011; Venturini et al. 2016), and as a result, these crossover times should be taken as upper bounds.

2.2. Accretion and Settling of Heavy Elements

Note that in the models of Pollack et al. (1996) it was assumed that all the added planetesimal material eventually sank to the core; here we relax that assumption. The accreted planetesimals are assumed to be composed of water (H_2O), rock (SiO_2), and organic material (CHON) in relative mass fractions of 0.4:0.3:0.3, respectively. The organic material is represented by hexacosane ($C_{26}H_{54}$), which is a paraffin-like substance. The accretion rate of planetesimals is given by the standard fundamental expression (e.g., Equation (1) of Movshovitz et al.), with the gravitational enhancement factor F_g given by Greenzweig & Lissauer (1992). We follow the trajectory of the planetesimals as they pass through the protoplanetary envelope. At each step of the trajectory we compute the motion of the planetesimals in response to gas drag and gravitational forces. The effects of heating, ablation, and fragmentation of planetesimals are also included. This calculation provides the distribution of heavy elements in the planetary envelope (see Pollack et al. 1996 for details).

When the heavy elements (planetesimals) dissolve, they are assumed to be fully vaporized, and then the amount of heavy material that remains at a given layer is limited by its vapor pressure and temperature. Following Iaroslavitz & Podolak (2007), we determine the partial pressure of the ablated heavy elements and compare it to the vapor pressure of the layer. If the partial pressure exceeds the vapor pressure, some of the accreted material is assumed to condense and settle to the layer below, leaving the (upper) layer fully saturated. The partial pressure of a given ablated material is calculated using the ideal gas law by

$$P = \frac{\Re \delta m T}{V \mu}, \tag{1}$$

where $\Re$ is the universal gas constant, δm is the mass ablated within the layer, T is the temperature, V is the volume of the layer (shell), and μ is the mean molecular weight of the material. We assume that the vapor pressure of a given substance above the critical temperature becomes infinite. The infinite vapor pressures allow any amount of the substance to be accommodated in the vapor without reaching saturation. The vapor pressure for the different materials is taken from Podolak et al. (1988) and Iaroslavitz & Podolak (2007):

$$P_{\rm vap}^{\rm water} = e^{-5640.34/T+28.867},\ T_{\rm crit} = 647.3\ {\rm K}, \tag{2}$$

$$P_{\rm vap}^{\rm CHON} = 6.46 \cdot 10^{13} e^{-12484.5/T},\ T_{\rm crit} = 843.4\ {\rm K}, \tag{3}$$

$$P_{\rm vap}^{\rm rock} = 10^{-24605/T+13.176},\ T_{\rm crit} = 4000\ {\rm K}. \tag{4}$$

The procedure is then repeated in each successive layer. If the heavy elements reach the innermost layer, they are added to the center of the planet, i.e., the core.

2.3. The Heavy-element Distribution

The heavy-element mass fraction (Z) at a given layer is calculated by

$$Z = \frac{M_{\rm SiO_2} + M_{\rm H_2O} + M_{\rm CHON}}{M_{\rm SiO_2} + M_{\rm H_2O} + M_{\rm CHON} + M_{\rm H+He}}, \tag{5}$$

where $M_{\rm SiO_2}$, $M_{\rm H_2O}$, $M_{\rm CHON}$, and $M_{\rm H+He}$ are the masses of rock, water, organics, and hydrogen+helium, respectively. In order to derive the Z-profile (heavy-element distribution) within the protoplanet, we first need to determine the mass distribution of the three different materials: rock (SiO_2), water (H_2O), and organics (CHON). The different vapor pressures of the different accreted materials lead to different mass distributions after settling is considered. Figure 1 shows the mass distributions of the various components at four different time steps for Model B. The mass distributions are shown before (green) and after (blue) settling is considered. Rock is represented by the dot–dashed curve, while organics and water are represented by the solid and dashed curves, respectively. The mass of hydrogen and helium (H+He) is represented by the thin gray curve.

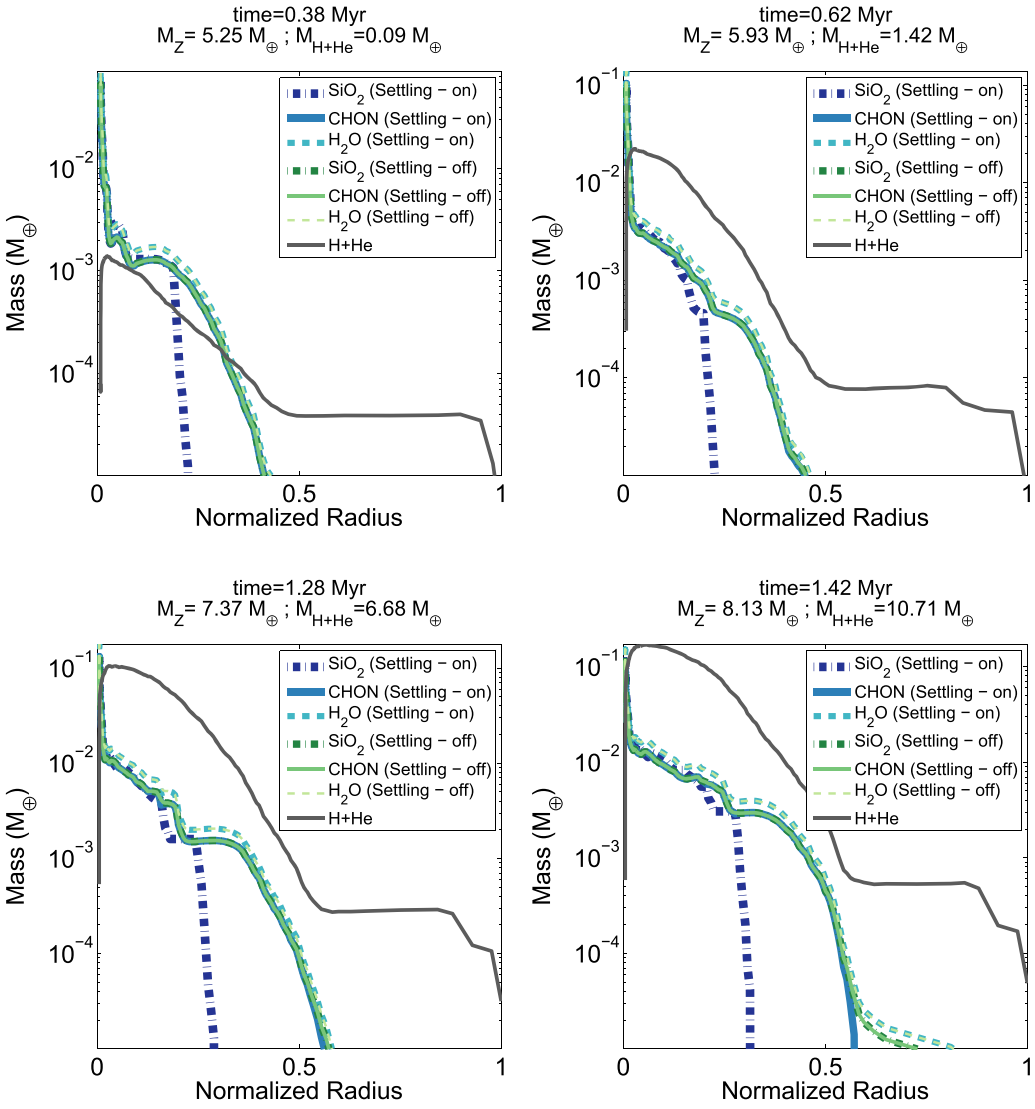

Figure 1. Mass distributions of the different materials vs. normalized planetary radius at various times for Model B. The blue and green curves represent the mass distributions before and after settling is considered, respectively (see the text for details).

Several conclusions can be drawn from the figure. First, in comparison to H+He, even before settling is applied, the heavy elements are more concentrated toward the planetary center. This is because planetesimals lose mass and break up only when the envelope's density and temperature are high enough for the planetesimals to experience sufficient gas drag. Second, after settling is considered, the distribution of the different materials becomes nonhomogeneous: while water and organics tend to remain where they are originally deposited, silicates settle toward the center. This may suggest that the (primordial) envelopes of giant planets are more enriched with volatiles, while the refractory materials are concentrated in the deep interior.

2.4. Convective Mixing and Equation of State

Although we find that the distribution of heavy elements due to planetesimal accretion and settling is inhomogeneous, convective mixing can homogenize the envelope's composition. The presence of convection in regions with composition gradients is determined by the ratio between the destabilizing temperature gradient and the stabilizing composition gradient (the Ledoux criterion); if the latter is dominant, the region is assumed to be radiative/conductive and no mixing occurs, although layered convection could develop in such regions (Vazan et al. 2015). The stability against convection in each layer accounting for the composition gradients using the Ledoux criterion is given by

$$\nabla - \nabla_{\rm ad} - \nabla_X < 0, \quad (6)$$

where $\nabla \equiv \frac{d\ln T}{d\ln P}$, $\nabla_{\rm ad}$ is the adiabatic gradient, and $\nabla_X \equiv \frac{\partial \ln T(p,\rho,X)}{\partial X_j} \cdot \frac{dX_j}{d\ln P}$. When convection is inefficient, $\nabla \sim \nabla_{\rm rad}$, where $\nabla_{\rm rad}$ is the radiative/conductive gradient.

In order to compute all the relevant physical properties that are required for the convection criterion calculation (e.g., ∇_X, $\nabla_{\rm ad}$, κ), we must use an equation of state (EOS). The EOS is calculated using the SCVH EOS tables by Saumon et al. (1995) for hydrogen and helium with an extension for low pressure and temperatures. Since there is no EOS available for organic materials, the heavy elements are represented by a mixture of H_2O and SiO_2 using the QEOS method (More et al. 1988). More details on the QEOS calculation can be found in Vazan et al. (2013) and references therein.

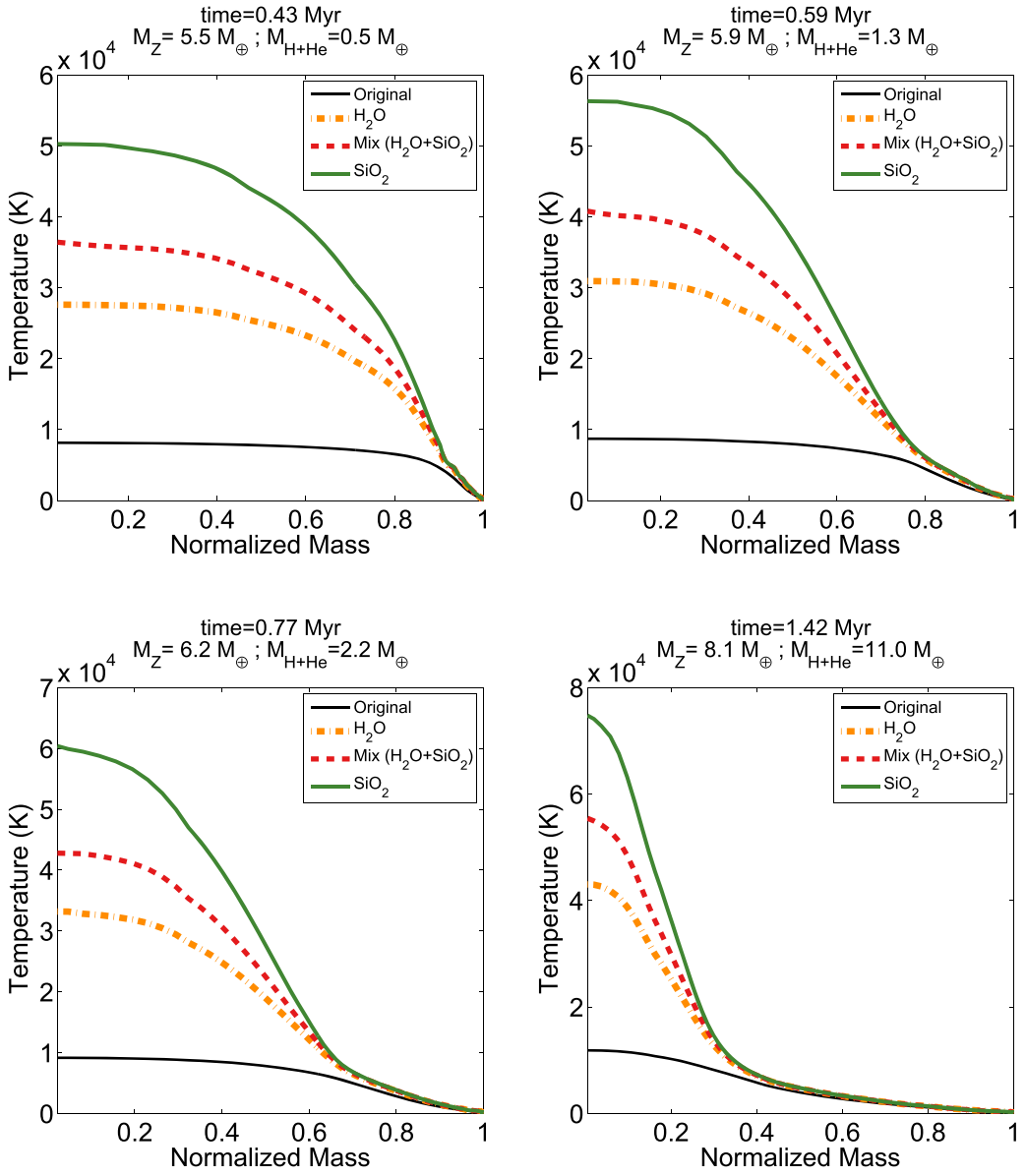

Figure 2. Temperature profile as a function of normalized mass for four different times for Model B. Shown are four different temperature profiles: the original temperature profile (without heavy elements; solid black), pure water (dot–dashed orange), mixture of water and silica (dashed red), and pure silica (solid green).

We assume that regions with shallow composition gradients (the outer layers) mix if they are unstable to convection according to the Ledoux criterion, resulting in a homogeneous composition with the average Z-value. The outermost regions of the protoplanet are not convective but radiative (Guillot et al. 1995), and they are too cold to maintain heavy elements in a gaseous phase. As a result, grains are likely to form and settle toward inner regions, where they evaporate and mix with the surrounding gas. In order to account for this effect, we settle the heavy material from atmospheric regions with temperatures. We take a critical temperature of 1500 K for the silicates and of 650 K for the water and organics (hexacosane). This results in two steps in the outer regions of the planet: the outermost region up to a temperature of 650 K is metal-free, and there is an intermediate layer of vapor water and organics. Temperatures higher then 1500K are sufficient to maintain the rock in vapor phase. The outermost part of the protoplanet is then depleted in heavy elements and has $Z \sim 0$. The heavy elements that were found to be in these outer regions are added to deeper regions, and their contribution to the local heavy-element concentration is included.

The original envelope's temperature (as well as density and pressure) is calculated assuming that all the heavy elements go to the center, and the envelope's composition is a mixture of hydrogen and helium in protosolar ratio, i.e., the hydrogen-to-helium ratio is set to be 0.705:0.275 (e.g., Bahcall et al. 1995). Since in our calculation the heavy elements can remain in the envelope, the contribution of the heavy materials to the envelope's temperature must be considered. In addition, because the temperature profile determines the efficiency of convection, it is important to understand how the heavy elements affect the envelope's temperature. Different materials have different effects on the temperature, and as a result, we compare four temperature profiles: the first is the original temperature profile assuming an H+He envelope, and the other three are the temperature profiles that are inferred when

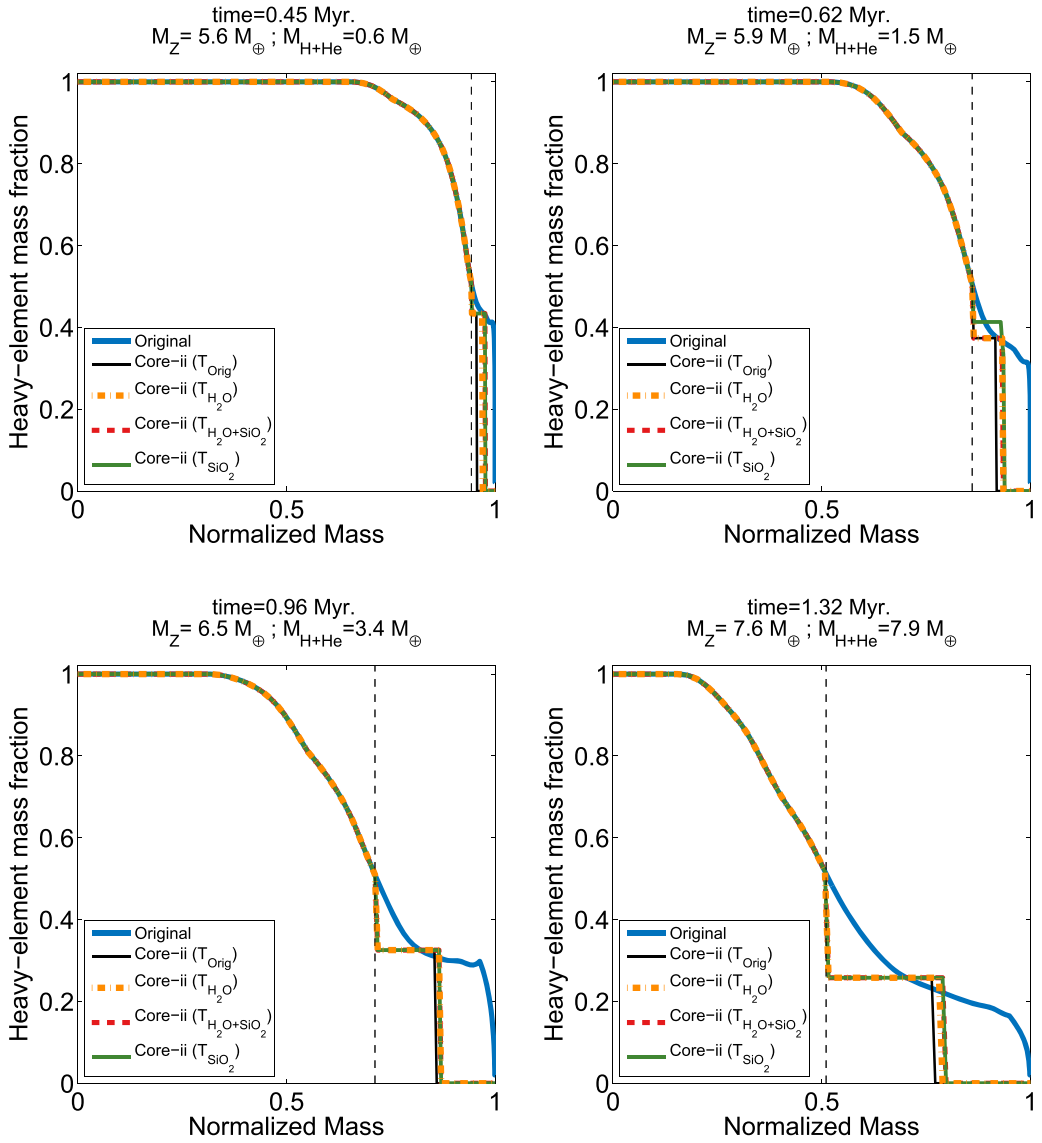

Figure 3. Heavy-element distribution as a function of normalized mass at different times for Model B when using the different temperature profiles for different compositions.

accounting for the effect of the heavy elements assuming three different compositions: pure SiO_2, pure H_2O, and an SiO_2–H_2O mixture. These calculations use the original temperature, pressure, and density of the envelope and the distribution of heavy material that is dissolved in the envelope (X, Y, Z). We then compute the modified temperature profiles that correspond to the original pressure of the envelope. The temperature as a function of normalized mass for different compositions is presented in Figure 2.

It is clear from the figure that the addition of heavy elements to the envelope increases its temperature, with SiO_2 having the largest effect. The increase in temperature is caused by the change in the opacity when the heavy elements are included. In the innermost regions, the opacity value can increase by about a factor of 100. As expected, the temperature profile of the SiO_2–H_2O mixture falls between the profiles of pure rock and pure water. We therefore suggest that the internal temperatures of young giant planets are higher than typically derived by formation models that do not account for this effect. Since the internal temperatures can reach well over 10^4 K, it is possible that the small inner core melts and mixes with the envelope, as we discuss below. Although the existence of heavy elements in the envelope leads to a significant increase in temperature, the *temperature gradient* remains about the same, and as a result, the identification of the convective regions in the envelope is not expected to change. The temperature gradient in the convection zones is the adiabatic gradient. In order to verify that, we derive the Z-profile for the different calculated temperature profiles and apply the convection criterion for these new conditions. The results are shown in Figure 3 for formation Model B. In this calculation the core is defined as the innermost region with heavy-element mass fraction larger than 0.5 (see the following section). Indeed, the figure suggests that the change of temperature and the assumed composition of the heavy elements do not affect the mixing pattern. This ensures that the heavy-element profiles we derive in this work are realistic, and they are not expected to differ much if other materials are assumed. In the following sections the heavy elements are represented by a mixture of water and silica (50%–50%).

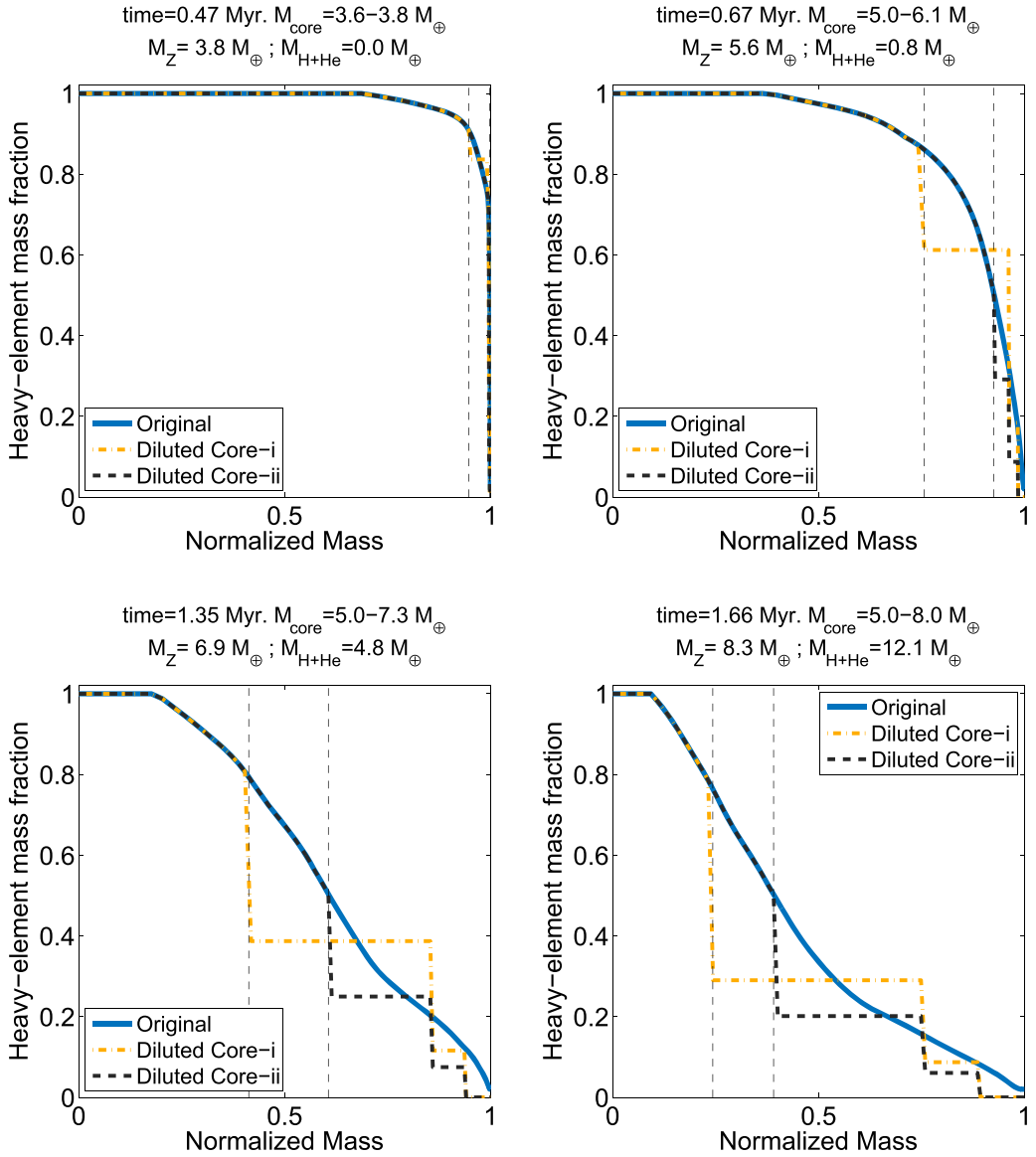

Figure 4. Distribution of the high-Z material (as a function of normalized mass) at different times for Model A: $\sigma = 6$ g cm^{-2}, planetesimal size = 100 km for the two core definitions. The dot–dashed orange and dashed black curves show the Z-profiles for Diluted Core-i and Diluted Core-ii, respectively. The core region is represented by the dashed black line.

2.5. The Definition of the Core

Defining the core of a giant planet is not trivial. Jupiter's core mass is typically inferred from structure models that fit the measured gravitational field of the planet (e.g., Guillot 2005). Typically, standard three-layer interior models infer a core mass between zero and $\sim$10 $M_\oplus$, while the total heavy-element mass is uncertain and is estimated to be between 10 and 40 $M_\oplus$ (Guillot 1999; Saumon & Guillot 2004; Nettelmann et al. 2008, 2012). Alternative models suggest a massive core (about 14–18 $M_\oplus$) and a smaller enrichment in heavy elements in Jupiter's gaseous envelope (Militzer et al. 2008; Hubbard & Militzer 2016). However, despite the accuracy of interior models, the chemical composition and physical state of the core cannot be inferred. Moreover, even if a core exists, it is not clear how distinct it is from the layers above it, although for simplicity, it is typically taken to be a separate region, and the core–envelope boundary (CEB) is assumed to have a density (and composition) discontinuity. It is also possible that the CEB is "bleary" (and therefore not well defined) and that the change in density (and composition) is more continuous. In that case, the core could be more extended and could even consist of some hydrogen and helium (Stevenson 1982).

The original formation models have a small primordial (solid) core in the early stages. The simulations begin with a Mars-size object that accretes planetesimals and gas. The actual core, however, is not modeled. The only thing that is followed is the increase in the core's mass due to the ongoing planetesimal accretion. The innermost region that is physically modeled is the bottom of the envelope, just above the core. Therefore, any possible interaction between the core and the surrounding gaseous envelope is neglected. As suggested by the formation models used in this work, once the core mass reaches $\sim$1–2 $M_\oplus$, the planetesimals dissolve in the envelope. This is in agreement with other giant planet formation models, such as the one presented by Pollack et al. (1996) and Venturini et al. (2016). If the core is defined as a pure heavy-element

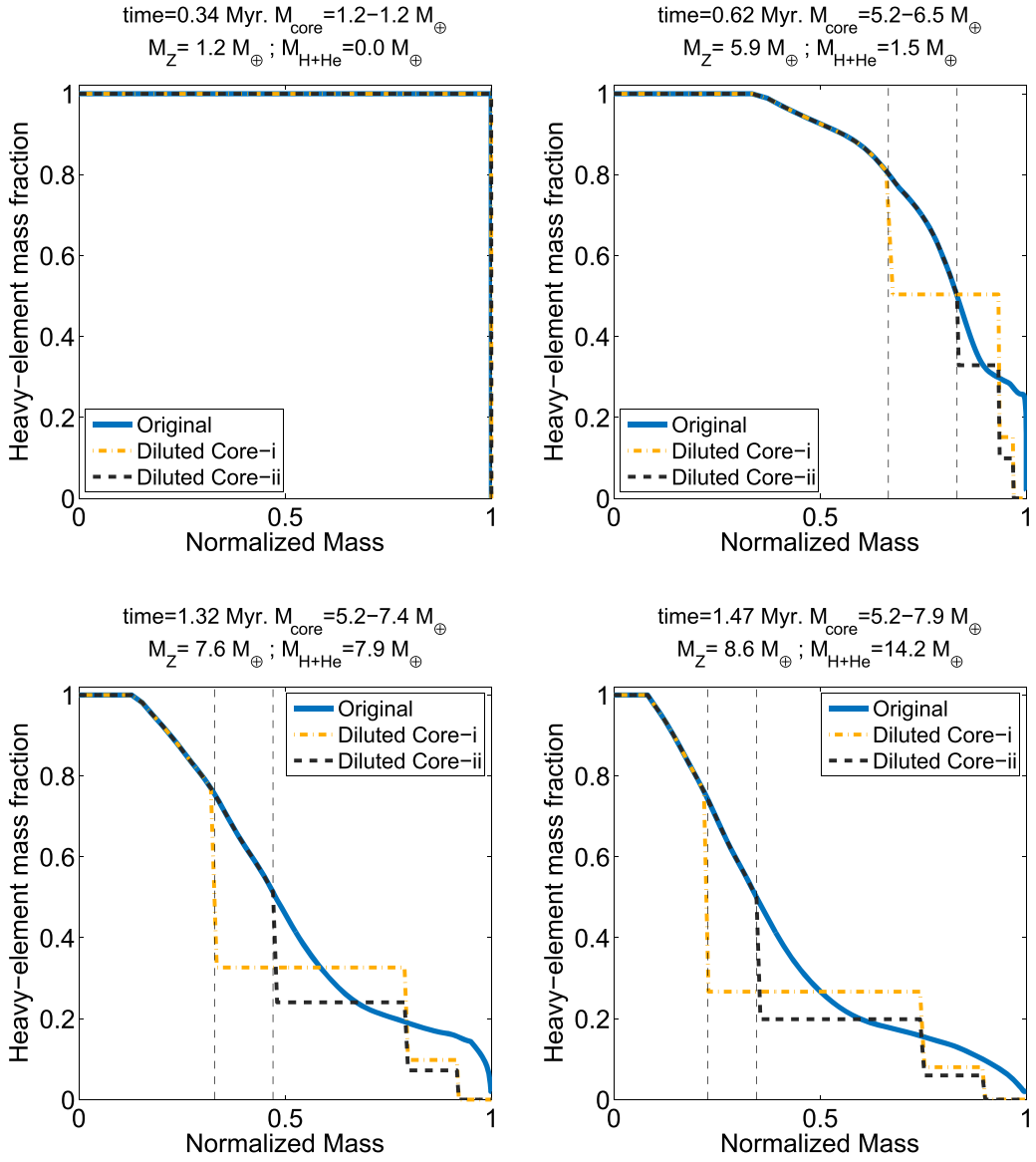

Figure 5. Same as Figure 4, but for Model B: $\sigma = 6$ g cm^{-2}, planetesimal size $= 0.5$ km.

region, the core mass is not expected to increase significantly, suggesting that Jupiter's core is smaller than the typical core masses inferred by *CA* models. Thus, as we discuss below, it may be that our perception of the core should be different (and less conservative), and that the cores of giant planets could be defined as the innermost region that is enriched with heavy elements. In this case, the core is more massive, larger, and diluted with light materials (i.e., H+He). Similar diluted core models for Jupiter have been considered by Fortney & Nettelmann (2010).

In this work the core is taken to be the innermost region with a heavy-element mass fraction (Z) that is larger than some critical value. We consider two critical values: Diluted Core-i with $Z \geqslant 0.9$, and Diluted Core-ii with $Z \geqslant 0.5$. In practice, due to the simplifications assumed for computing the disruption and mixing of the accreted material, it can happen that during the runaway gas accretion phase, the Z-profiles dilute too much. This causes the region of $Z \geqslant Z_{\rm crit}$ to shrink. However, this is a numerical artifact, because the planetesimal disruption model assumes that the envelope is metal-free. In reality, once a steep Z-profile exists in the envelope, the additional accretion of H+He should stay mainly on the top of the planet, leading to an onion-like structure (Stevenson 1982). Following this argument, and in order to not introduce a numerical bias in the mass of the core, we add, to the region of $Z \geqslant Z_{\rm crit}$, the necessary layers to the core region in order to reach (at least) the same mass of core we had in the previous time step. As we show below, under our core definition, the core is not necessarily distinct from the envelope, due to the existence of composition gradients within the planet. This is rather different from the "standard" view of Jupiter's core as a pure-Z region and the existence of a density discontinuity between the core and the envelope.

The rate of solid accretion during the phase of runaway gas accretion is not well understood. After crossover is reached, the protoplanet starts to accrete gas rapidly, and the planetary composition from this point on depends on the composition of the accreted gas and of the planetesimal accretion rate during this formation phase; both are poorly known (e.g., Alibert et al. 2005; Lissauer et al. 2009; Helled & Lunine 2014). As a

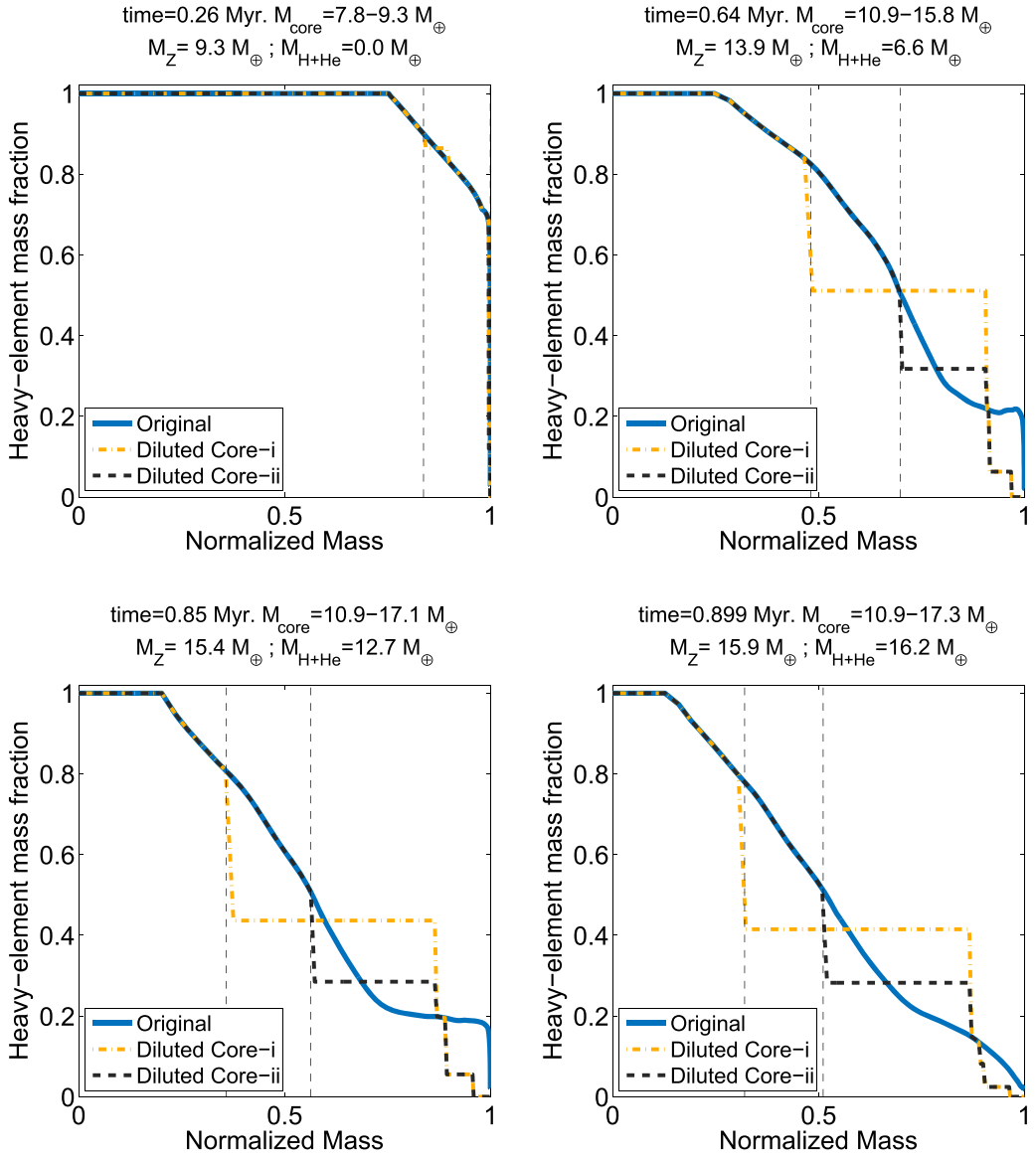

Figure 6. Same as Figure 4, but for Model C: $\sigma = 10$ g cm^{-2}, planetesimal size $= 1$ km.

result, more robust predictions in terms of composition and internal structure can be made up to the crossover time. Nevertheless, in Section 3.2 we also present calculations in which the planetary formation goes all the way to a Jupiter mass, assuming that the accreted gas has a solar composition and that no planetesimals are accreted during runaway gas accretion. Thus, on the contrary, if during runaway accretion a large fraction of heavy elements were accreted, the final composition of the envelope would be supersolar, and in that case our results should be taken as a lower bound for the envelope (atmospheric) enrichment of Jupiter. In addition, it is possible that during rapid gas accretion some material from the outer part of the core will mix into the envelope and thus reduce the mass of the core. This, however, must be modeled in detail before conclusions on core erosion during formation can be made.

3. Results

Figures 4–7 show the distributions of the high-Z material (in mass fraction, Z) as a function of normalized mass at different times for the four different formation models. The blue curve represents the original distribution of heavy elements after settling is also included, while the dot–dashed orange and dashed black curves show the Z-profiles after convective mixing is considered for Diluted Core-i and Diluted Core-ii, respectively. The time, total mass of heavy elements (M_Z), total mass of hydrogen and helium ($M_{\rm H+He}$), and calculated core mass ($M_{\rm core}$) are given in the header of each panel. It can be seen that at early times, the protoplanet is composed of mostly heavy elements, while only the outermost layers are depleted in heavy elements (blue curve). At each time step, we first derive the composition gradient, and then the innermost layers with a heavy-element mass fraction Z that is larger than the critical value are added to core, and the rest of the envelope is allowed to mix according to the Ledoux criterion. As discussed above, if the mass of the core region is smaller than the core mass calculated in the previous model, we add a few layers above the core region until the correct core mass is reached. Otherwise, we simply collect all the layers with heavy-element mass fraction that is larger than the critical value, and we derive the new core mass. As time progresses, the heavy-element

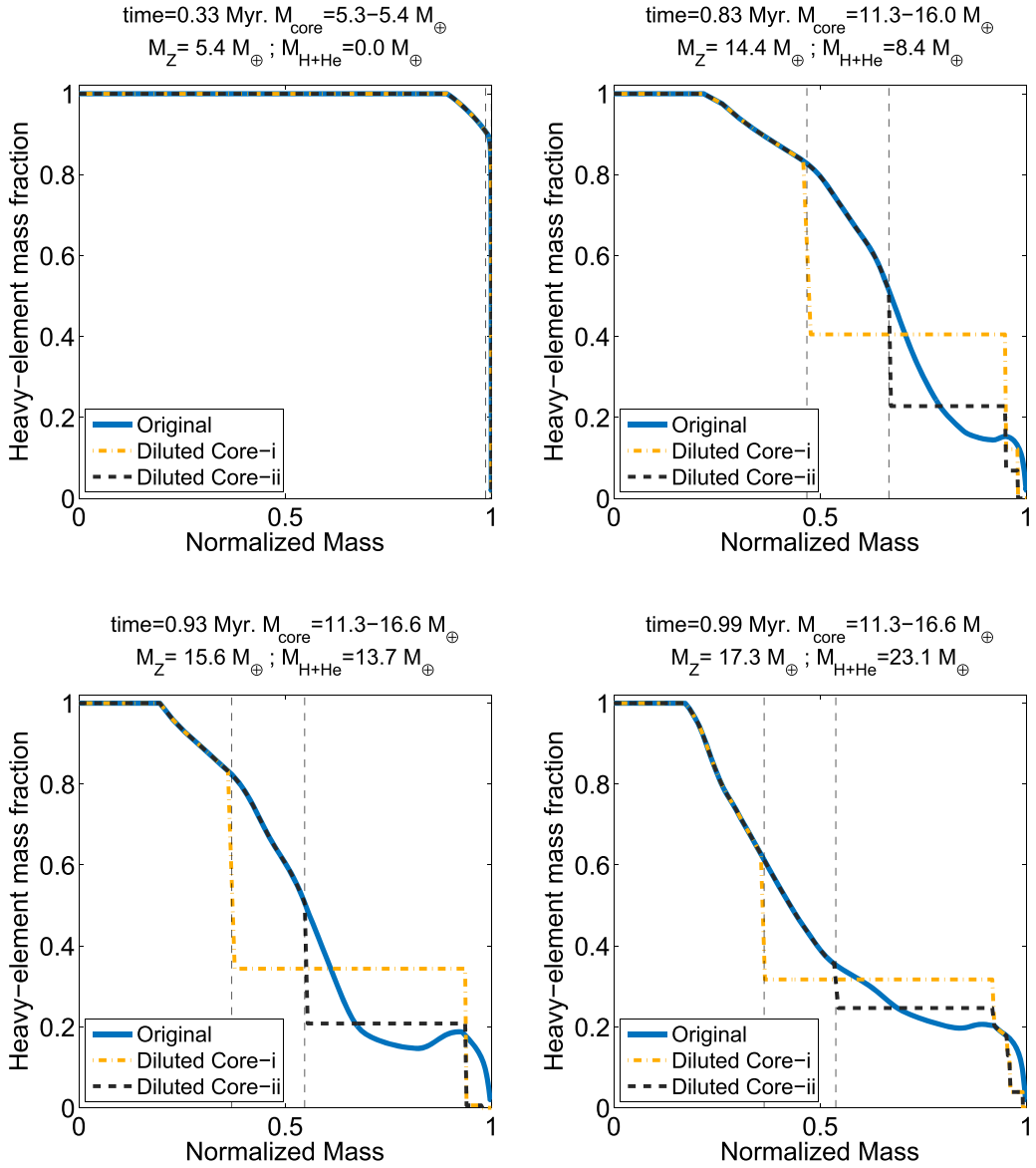

Figure 7. Same as Figure 4, but for Model D: $\sigma = 10\ \mathrm{g\ cm^{-2}}$, planetesimal size = 100 km.

Table 2
Inferred Core Mass and Modified Crossover Time ($M_{\mathrm{Core}} = M_{\mathrm{H+He}}$ Instead of the Original $M_Z = M_{\mathrm{H+He}}$) for the Different Formation Models and Various Core Definitions

Formation Model	Diluted Core-i		Diluted Core-ii	
	M_{core}	t_{cross}	M_{core}	t_{cross}
	($M_\oplus$)	(Myr)	($M_\oplus$)	(Myr)
Model A	4.96	1.36	7.57	1.53
Model B	5.21	1.16	7.43	1.30
Model C	10.86	0.80	17.32	0.90
Model D	11.27	0.88	16.64	0.95

distribution becomes more gradual, but in the inner region the gradient is steep enough to inhibit convective mixing. In all cases, the bottom of the envelope reaches very high temperatures (over 10^4 K), due to the existence of heavy elements.

It is interesting to note that for the formation models with $\sigma = 6\ \mathrm{g\ cm^{-2}}$ the distribution of the heavy elements is more gradual than the ones for the case of $\sigma = 10\ \mathrm{g\ cm^{-2}}$. This seems to be linked to the total formation timescale, in particular, the length of the slow gas accretion phase. When $\sigma = 10\ \mathrm{g\ cm^{-2}}$, the planetary structure is more similar to a standard core+envelope structure. Model D is the closest to having a core+envelope structure since the solid-surface density is high, and the planetesimals are large, so even with dissolution of planetesimals in the envelope, most of the accreted heavy elements tend to be in the deep interior.

For the case of Diluted Core-ii, the calculated core mass is larger, especially at later times, but the core's density is lower because in this case the core consists of a larger fraction of hydrogen and helium. In addition, the core has a gradual change in the heavy-element mass fraction, which is decreasing toward the core's outer region. Both Diluted Core-i and Diluted

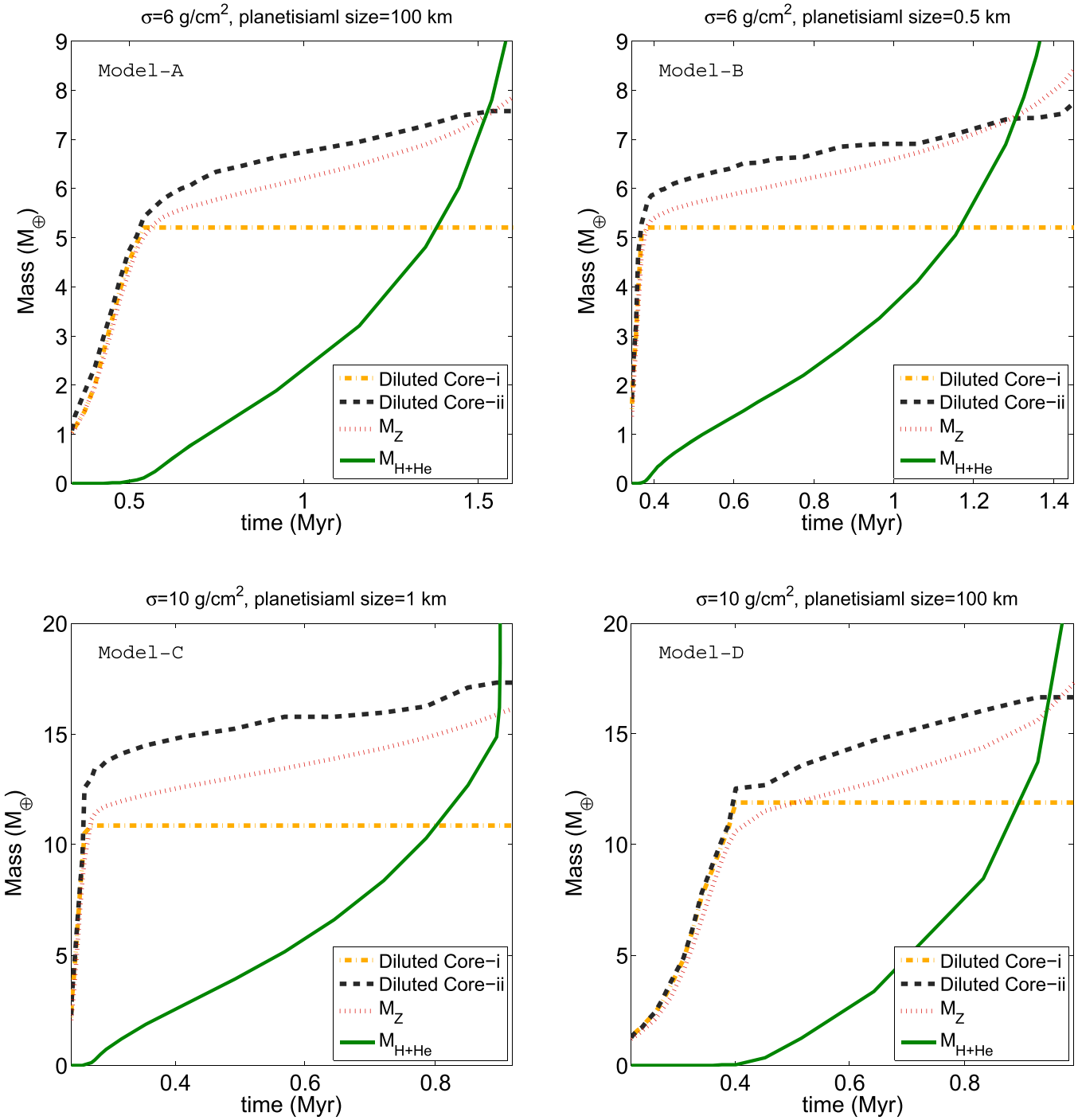

Figure 8. Evolution of the planetary mass for the four formation models. The masses of H+He and heavy elements are represented by the solid green and dotted red lines, respectively. In addition, the dot–dashed orange and dashed black curves correspond to Diluted Core-i and Diluted Core-ii, respectively. The gaseous (H+He) mass, total heavy-element mass, and core mass at crossover time are listed in Table 2.

Core-ii consist of hydrogen and helium and have composition gradients. This suggests that the cores of giant planets can have very different physical properties (mass, composition, radius, etc.) and can be more complex than the standard cores that are typically assumed.

The crossover times and the corresponding inferred core masses are summarized in Table 2 and are denoted by $t_{\rm cross}$ and $M_{\rm cross}$. As the planetesimal's size increases, the time to reach crossover increases as well, while for higher solid-surface densities, the formation process is shorter and therefore the time to crossover decreases. This is because small planetesimals tend to form smaller cores, and high solid-surface densities correspond to higher solid accretion rates, which reduce the formation timescale. It should be kept in mind, however, that the crossover times presented here correspond to formation models that assume a metal-free envelope, and the actual crossover time could be significantly shorter when the heavy elements in the envelope are included (e.g., Hori & Ikoma 2011; Venturini et al. 2016). Based on the work of Venturini et al. (2016), $t_{\rm cross}$ is expected to change by a factor

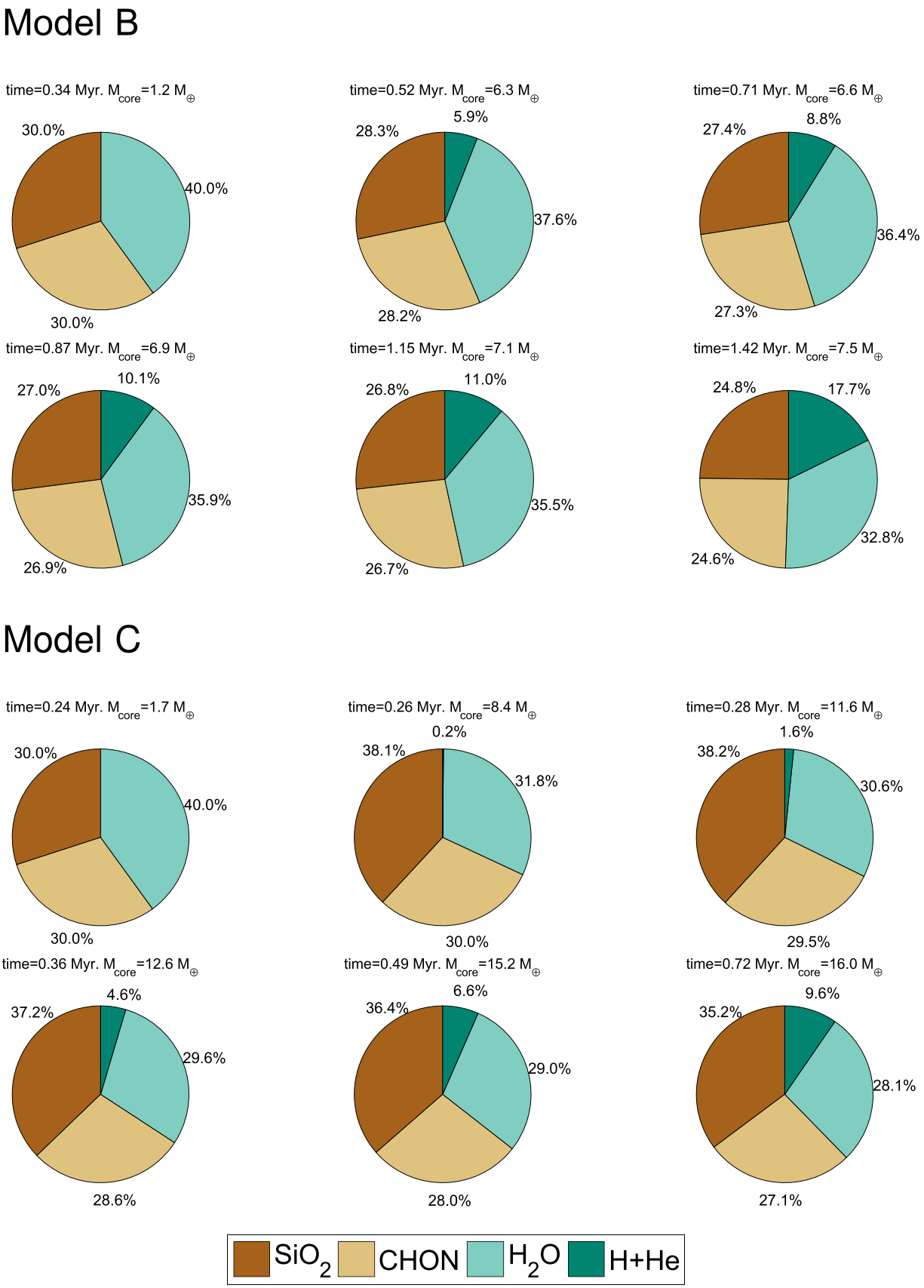

Figure 9. Derived core composition at various times for Models B and C. The core is defined as the innermost region with $Z > 0.5$ (Diluted Core-ii). SiO_2, CHON, H_2O, H+He are represented by the brown, beige, blue, and turquoise colors, respectively.

Table 3
Composition of Jupiter's Core at Crossover for Diluted Core-i (top) and Diluted Core-ii (Bottom) for the Four Formation Models (see the Text for Details)

Formation Model	H + He (%)	SiO_2 (%)	H_2O (%)	CHON (%)
Diluted Core-i				
Model A	4.3	28.7	38.3	28.7
Model B	3.8	28.9	38.5	28.8
Model C	2.3	37.6	30.8	29.3
Model D	3.8	36.6	30.7	28.9
Diluted Core-ii				
Model A	18.1	24.6	32.7	24.6
Model B	19.0	25.7	34.0	25.5
Model C	12.2	34.3	27.2	26.3
Model D	9.9	34.8	28.3	27.0

of a few. The derived core masses are between about 5 and 17 $M_\oplus$, with the core mass depending on the critical value that is applied, as well as on the assumed planetesimal size and solid-surface density. These values are significantly higher than the $\sim 2\ M_\oplus$ that is expected from a pure heavy-element core, and at the same time also different from a massive core of a similar mass assuming that all the accreted planetesimals go to the center. Thus, these cores are massive, are extended, have compositional gradients, and are not pure-*Z*.

Figure 8 shows the envelope's (H+He) mass and the core masses for the two core cases as a function of time until crossover is reached for the four formation models. As can be seen from the figure, the calculated core mass is typically smaller than the total heavy-element mass for Diluted Core-i, but is larger than the total heavy-element mass for Diluted Core-ii. For the models with $\sigma = 6\ \mathrm{g\,cm^{-2}}$, the derived core masses are smaller by more than a factor of two than for the cases with $\sigma = 10\ \mathrm{g\,cm^{-2}}$. Another interesting thing to note is that the H+He curve and the curve of Diluted Core-ii meet at about the same time as the original M_Z; although this may suggest that the crossover time is not expected to change much, it is clear that the core properties in our models are very different since Core-ii can contain a large fraction of H+He near crossover, as we show in the following section.

3.1. The Composition of the Core

Since in our analysis the core is defined by a critical *Z*-value of the innermost layers, we can derive the core's composition as a function of time. Figure 9 shows the derived core composition at various times. The top and bottom panels correspond to formation Models B and C, respectively. We find that as time progresses, the mass of the core and the percentage of hydrogen and helium increase. While the initial core has a similar composition to that of the planetesimals, as it grows in mass, the overall composition changes because of the different distributions of the materials when settling is considered. The core is found to consist of a larger fraction of rock compared to water and CHON in Models C and D (formation models with $\sigma = 10\ \mathrm{g\,cm^{-2}}$) and has almost the initial proportions for Models A and B (formation models with $\sigma = 6\ \mathrm{g\,cm^{-2}}$). The derived core compositions for the four formation models at crossover time are listed in Table 3.

It is interesting to note that although the derived core masses are different, the composition of the core is about the same. Moreover, we find that the core's composition is more sensitive to the assumed solid-surface density than to the planetesimals' size. In addition, the difference between the cases of Diluted Core-i and Diluted Core-ii is not very large, which suggests that there are not many internal layers with heavy-element fractions between $Z \geqslant 0.9$ and $Z \geqslant 0.5$, i.e., the composition gradient is relatively steep. This is indeed demonstrated in the figures that show the distribution of heavy elements within the planets at various times.

3.2. Modeling the Formation up to a Jupiter Mass

In the previous sections, the formation of Jupiter was followed only up to the crossover time (i.e., when $M_{\mathrm{H+He}} = M_Z$ in the original formation models). Here we follow the planetary formation including runaway gas accretion up to the stage when Jupiter's mass is reached for Models A and C. The distribution of the heavy elements at various times is shown in Figures 10 and 11, respectively. The accreted gas is assumed to have a protosolar composition. We consider the two different core definitions. After crossover is reached, the gas accretion rate increases rapidly and the protoplanet accretes large amounts of gas (H+He). The total mass of the planet increases rapidly, and the core becomes very small relative to the envelope. The most massive cores we derive are for Model C, with a mass of about 13 and 17 $M_\oplus$ for the cases of Diluted Core-i and Diluted Core-ii, respectively.

As can be seen from the figures, when we allow the outer regions to mix by convection, the original heavy-element distribution (blue curve) can break into a few different regions, with the outermost regions becoming nearly metal-free as a result of grain settling. Toward the end of the formation, convective regions are found to be separated by stable (radiative/conductive) layers, resulting in "stairs." These stairs could be a numerical artifact, but they might also indicate that giant planets could have several convective regions that are separated by thin radiative layers (see, e.g., Guillot et al. 1994). Regions with a high fraction of heavy elements that are found to be stable against convection could in principle develop layered convection (e.g., Leconte & Chabrier 2012; Vazan et al. 2016). The importance of the primordial internal structure of Jupiter on its planetary evolution has been recently investigated by our group (see Vazan et al. 2015, 2016), and we hope to combine these two aspects self-consistently in the future. In the innermost regions with the steep composition gradients, slow mixing could essentially occur by double-diffusive/layered convection at later stages in the planetary evolution. We therefore suggest that future giant planet formation and evolution models should account for this effect, as it can change the predicted distribution of heavy elements in proto-Jupiter and the cooling history of the planet (e.g., Vazan et al. 2016).

Figure 12 shows the final models for Diluted Core-i and Diluted Core-ii for Model A (top) and Model C (bottom). The "final model" in our case is defined by the mass of the planet,

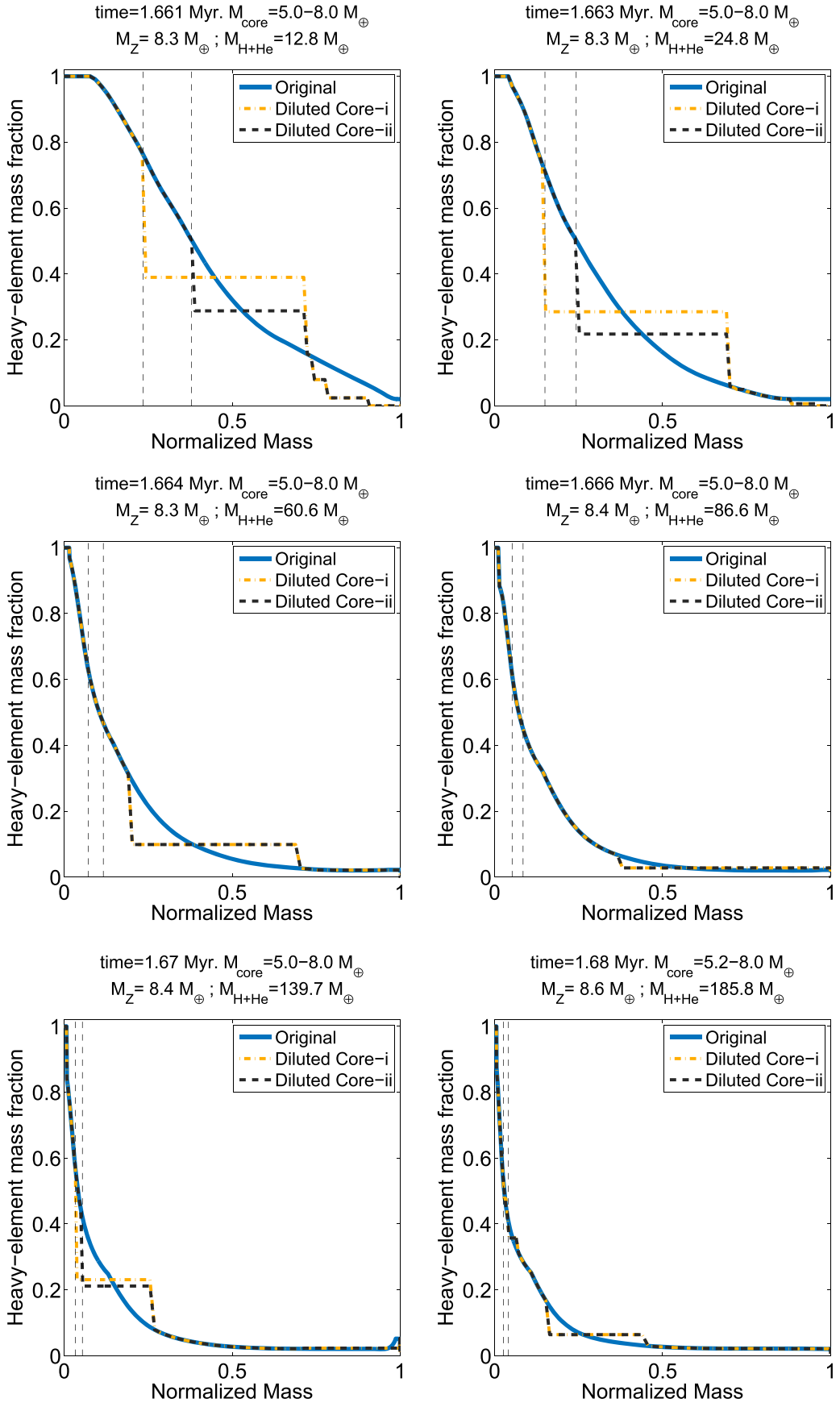

Figure 10. Distribution of the high-Z material vs. normalized mass at different times for Model A for Diluted Core-i (dot–dashed orange) and Diluted Core-ii (dashed black) during phase 3.

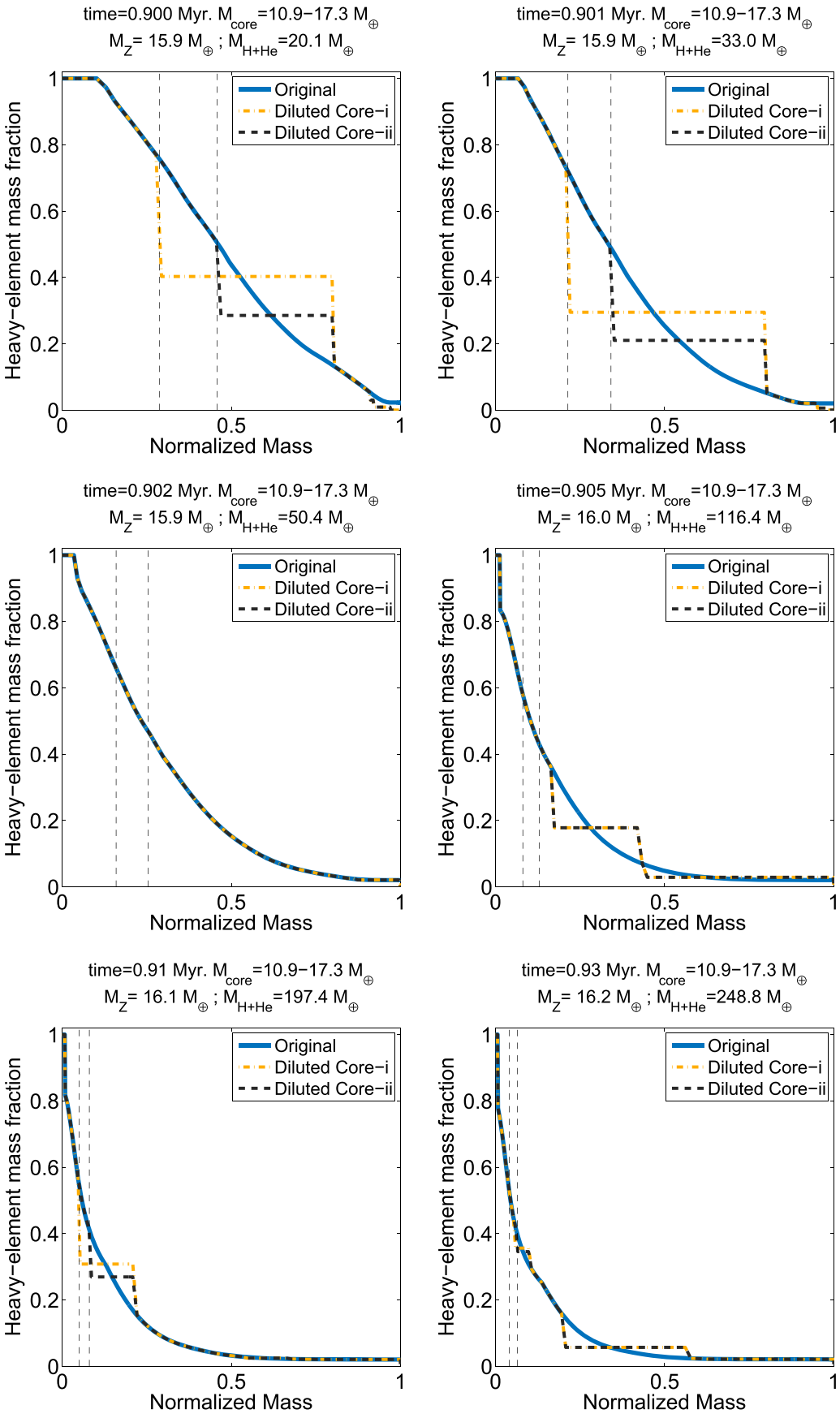

Figure 11. Same as Figure 10, but for Model C.

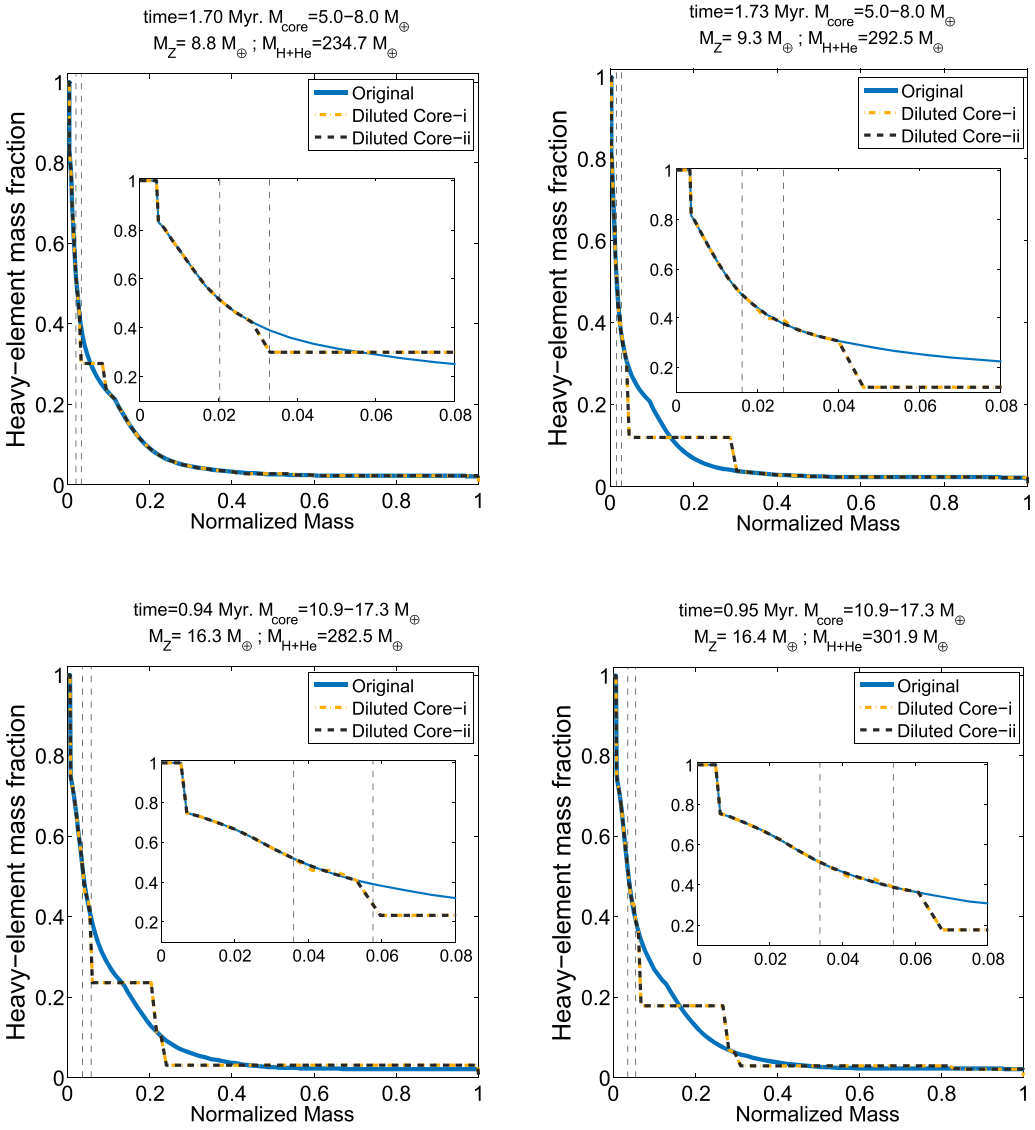

Figure 12. Distribution of heavy elements in models of proto-Jupiter as they approach the final mass of 1 Jupiter mass at the end of rapid gas accretion. Top panels: Model A; bottom panels: Model C. Dot–dashed orange lines: Diluted Core-i; dashed black lines: Diluted Core-ii.

i.e., when the planet reaches a mass of $\sim 1 M_J$ and gas accretion is terminated. In both cases, there is an inner region with a composition gradient (above the small primordial core). While this region is of the order of 5% of the planet's radius, this configuration can affect the long-term evolution of the planet. The envelope above the core is found to be fully mixed, suggesting an adiabatic outer envelope. The inner regions with composition gradients can mimic the existence of a massive core. As a result, this option should be accounted for when inferring Jupiter's core mass from gravitational data.

4. Discussion and Conclusions

We present a calculation of Jupiter's formation and primordial internal structure in the CA model, including the enrichment of the planetary envelope as a result of planetesimal accretion and settling. We follow the distribution of heavy elements within the protoplanet during its growth, taking into account the redistribution of heavy elements due to settling and convective mixing in the outer envelope. It is found that a substantial amount of the ablated heavy material remains in the planetary envelope. Since different assumed solid-surface densities and planetesimal sizes lead to different core masses, it is clear that the birth environment of the planet has an impact on its final internal structure.

If the core is defined by a pure heavy-element region that is not interacting with the enriched envelope, Jupiter's core is predicted to have a mass of $\sim$1–2 $M_\oplus$. After that core mass is reached, the accreted planetesimals dissolve in the envelope. Here, we consider an alternative definition of Jupiter's core, accounting for two different critical values for Z, and investigate how they affect the predicted internal structure and core mass of proto-Jupiter. We find that under the Diluted Core-ii definition Jupiter's core is massive ($\sim$7–17 $M_\oplus$) but also consists of a non-negligible fraction of H+He. Naturally, when the core is defined by $Z > 0.5$, the inferred core mass is larger, and the core is more extended and has larger fractions of H+He. At crossover, the fraction of H+He for the core definition of $Z > 0.9$ is typically 2%–4%, and in the case of $Z > 0.5$, it is 10%–18%. Our analysis suggests that traditional planet formation models considering a heavy-element core surrounded by an H+He envelope are oversimplified, and

future formation (and structure) models should account for the existence of heavy elements in the envelope and their distribution self-consistently. This will lead to a more accurate prediction of the primordial internal structure of giant planets and, in particular, their core masses. We suggest that a natural next step is to follow the evolution of the planet and investigate whether the composition gradients will persist in Jupiter today (see Vazan et al. 2016).

While in most CA models the terms "heavy material" and "core" are essentially the same, we show that there is an important difference between the two, because most of the accreted heavy elements remain in the planetary envelope, and the core mass is significantly smaller than the total heavy-element mass. When convective mixing is considered, we find that the heavy elements are homogeneously distributed along the envelope. Thus, the innermost regions that have a steep enough composition gradient can remain stable against convection. These regions can also consist of hydrogen and helium and could be viewed as "extra-extended cores." The "extended cores" are of the order of 20 $M_{\oplus}$ in mass, but with lower density than that of a pure-Z core, due to the existence of H+He. Such a core should be considered in future internal structure models of Jupiter. The results of this work are relevant for the data interpretation from the *Juno* (NASA) mission to Jupiter. We suggest that Jupiter's core can be significantly smaller than predicted by standard core accretion models. At the same time, we also find that the innermost region of Jupiter can be enriched in heavy elements and mimic a massive core, with the difference that the core is larger and has a relatively low mean density. We hope that with *Juno*'s accurate gravitational measurements it will be possible to discriminate between the no/small core case and the extended massive (but not very dense) core case for Jupiter. Since our model suggests that composition gradients may exist in Jupiter's deep interior, such a (nonadiabatic) configuration should be considered in structure models. A nonadiabatic interior can affect the temperature profile within the planet and the efficiency of convection.

Our study emphasizes the importance of determining the heavy-element accretion rate during runaway gas accretion. The predicted composition of Jupiter (and giant planets in general) depends on the *assumed* gas composition and the solid accretion rate that is expected during runaway gas accretion. If during runaway a significant amount of heavy elements are accreted onto the planet, the composition of the outer envelope could be enriched as well. It is therefore extremely important to determine the heavy-element accretion rate during the last stages of giant planet formation, since it is directly linked to the prediction of the planetary composition (see Helled & Lunine 2014 and references therein for details).

The work presented here should be taken only as a first step toward more advanced and detailed investigations of Jupiter's formation and primordial internal structure. It is clear that the existence of heavy elements in the envelope can affect the growth history of giant planets, the physical properties of the envelope, and the predicted primordial internal structure (e.g., Hori & Ikoma 2011; Venturini et al. 2016), and these should be simulated and included in future giant planet formation models. Future studies could also include the impact of the heavy elements on the (gas+dust) opacity in the envelope, as well as re-condensation of the heavy elements in the envelope and the formation of clouds for various species, and the possibility of layered convection in regions where composition gradients exist. Moreover, this work has not included miscibility of the materials in hydrogen (e.g., Wilson & Militzer 2012; Soubiran & Militzer 2015). This could also affect the evolution of the planet and the predicted internal structure. Finally, our study demonstrates the importance of simulating the core in more detail. It would be desirable to model the core using physical equations of state and to investigate the core–envelope interaction. A more detailed analysis of the core's physical properties, its cooling rate, and the properties of the core–envelope boundary are crucial for constraining the internal structure of Jupiter. Such studies can put tighter limits on the predicted core mass (and physical properties) of Jupiter's primordial core.

We thank D. Stevenson, A. Vazan, A. Kovez, J. Venturini, and M. Podolak for valuable discussions and suggestions. R.H. acknowledges support from the Israel Space Agency under grant 3-11485 and from the United States—Israel Binational Science Foundation (BSF) under grant 2014112. P.B. received support from a grant from the NASA Origins program.

References

Alibert, Y., Mordasini, C., Benz, W., & Winisdoerffer, C. 2005, A&A, 434, 343
Bahcall, J. N., Pinsonneault, M. H., & Wasserburg, G. J. 1995, RvMP, 67, 781
Buhler, P. B., Knutson, H. A., Batygin, K., et al. 2016, ApJ, 821, 26
Fortney, J. J., & Nettelmann, N. 2010, SSRv, 152, 423
Greenzweig, Y., & Lissauer, J. 1992, Icar, 110, 440
Guillot, T. 1999, Icar, 47, 1183
Guillot, T. 2005, AREPS, 33, 493
Guillot, T., Chabrier, G., Gautier, D., & Morel, P. 1995, ApJ, 450, 463
Guillot, T., Chabrier, G., Morel, P., & Gautier, D. 1994, Icar, 112, 354
Helled, R., Bodenheimer, P., Podolak, M., et al. 2014, in Protostars and Planets VI, ed. H. Beuther, R. S. Klessen, C. P. Dullemond, & T. Henning (Tucson, AZ: University of Arizona Press), 643
Helled, R., & Lunine, J. 2014, MNRAS, 441, 2273
Hori, Y., & Ikoma, M. 2011, MNRAS, 416, 1419
Hubbard, W. B., & Militzer, B. 2016, ApJ, 820, 80
Iaroslavitz, E., & Podolak, M. 2007, Icar, 187, 600
Kramm, U., Nettelmann, N., Fortney, J. J., Neuhäuser, R., & Redmer, R. 2012, A&A, 538, 146
Leconte, J., & Chabrier, G. 2012, A&A, 540, A20
Lissauer, J., Hubickyja, O., D'Angelo, G., & Bodenheimer, P. 2009, Icar, 199, 338
Militzer, B., Hubbard, W. B., Vorberger, J., Tamblyn, I., & Bonev, S. A. 2008, ApJL, 688, L45
More, R. M., Warren, K. H., Young, D. A., & Zimmerman, G. B. 1988, PhFl, 31, 3059
Movshovitz, N., Bodenheimer, P., Podolak, M., & Lissauer, J. J. 2010, Icar, 209, 616
Nettelmann, N., Becker, A., Holst, B., & Redmer, R. 2012, ApJ, 750, 52
Nettelmann, N., Holst, B., Kietzmann, A., et al. 2008, ApJ, 683, 1217
Podolak, M., Pollack, J. B., & Reynolds, R. T. 1988, Icar, 73, 163
Pollack, J. B., Hubickyj, O., Bodenheimer, P., et al. 1996, Icar, 124, 62
Saumon, D., Chabrier, G., & van Horn, H. M. 1995, ApJ, 99, 713
Saumon, D., & Guillot, T. 2004, ApJ, 609, 1170
Soubiran, F., & Militzer, B. 2015, ApJ, 806, 228
Stevenson, D. 1982, P&SS, 30, 755
Vazan, A., Helled, R., Kovetz, A., & Podolak, M. 2015, ApJ, 803, 32
Vazan, A., Helled, R., Podolak, M., & Kovetz, A. 2016, ApJ, 829, 118
Vazan, A., Kovetz, A., Podolak, M., & Helled, R. 2013, MNRAS, 434, 3283
Venturini, J., Alibert, Y., & Benz, W. 2016, A&A, 596, 90
Wilson, H., & Militzer, B. 2012, PhRvL, 108, 111101